AIMS Mathematics, 9(4): 10185–10207.
DOI: 10.3934/math.2024498
Received: 21 January 2024
Revised: 29 February 2024
Accepted: 06 March 2024
Published: 14 March 2024

https://www.aimspress.com/journal/Math

Research article

An enhanced tunicate swarm algorithm with deep-learning based rice seedling classification for sustainable computing based smart agriculture

Manal Abdullah Alohali[1], Fuad Al-Mutiri[2], Kamal M. Othman[3,*], Ayman Yafoz[4], Raed Alsini[4] and Ahmed S. Salama[5]

[1] Department of Information Systems, College of Computer and Information Sciences, Princess Nourah bint Abdulrahman University, P.O. Box 84428, Riyadh 11671, Saudi Arabia
[2] Department of Mathematics, Faculty of Sciences and Arts, King Khalid University, Muhayil Asir, Saudi Arabia
[3] Department of Electrical Engineering, College of Engineering and Islamic Architecture, Umm Al-Qura University, Makkah, Saudi Arabia
[4] Department of Information Systems, Faculty of Computing and Information Technology, King Abdulaziz University, Jeddah, Saudi Arabia
[5] Department of Electrical Engineering, Faculty of Engineering & Technology, Future University in Egypt, New Cairo 11845, Egypt

* **Correspondence:** Email: Kmothman@uqu.edu.sa.

Abstract: Smart agricultural techniques employ current information and communication technologies, leveraging artificial intelligence (AI) for effectually managing the crop. Recognizing rice seedlings, which is crucial for harvest estimation, traditionally depends on human supervision but can be expedited and enhanced via computer vision (CV). Unmanned aerial vehicles (UAVs) equipped with high-resolution cameras bestow a swift and precise option for crop condition surveillance, specifically in cloudy states, giving valuable insights into crop management and breeding programs. Therefore, we improved an enhanced tunicate swarm algorithm with deep learning-based rice seedling classification (ETSADL-RSC). The presented ETSADL-RSC technique examined the UAV images to classify them into two classes: Rice seedlings and arable land. Initially, the quality of the pictures could be enhanced

by a contrast limited adaptive histogram equalization (CLAHE) approach. Next, the ETSADL-RSC technique used the neural architectural search network (NASNet) method for the feature extraction process and its hyperparameters could be tuned by the ETSA model. For rice seedling classification, the ETSADL-RSC technique used a sparse autoencoder (SAE) model. The experimental outcome study of the ETSADL-RSC system was verified for the UAV Rice Seedling Classification dataset. Wide simulation analysis of the ETSADL-RSC model stated the greater accuracy performance of 97.79% over other DL classifiers.

Keywords: smart agriculture; crop monitoring; rice seedling; computer vision; image classification; deep learning
Mathematics Subject Classification: 11Y40

1. Introduction

Nowadays, advanced remote sensing (RS) has turned out to be a renowned technique for acquiring high-throughput and large-scale crop data in plant phenotypes, as it can capture multi-temporal RS images (RSI) of crop growth on demand [1]. Generally, the three widely used RS platforms are UAV-related, satellite, and ground platforms [2]. Of these, the UAV-related platform is utilized for making frequent flight experimentations when and where required, which allows for monitoring high-resolution spatial paradigms for capturing a considerable amount of multitemporal highest-definition images for monitoring crop [3]. Additionally, their high flexibility and affordable rate make UAV-related stages prevalent in the research field, and several new applications for UAV image analysis were devised. Such new applications include vegetation monitoring, mapping of archaeological places, oil and gas pipeline observation, urban site analysis, object detection, and disaster management [4]. With the growth of computational power and vast amount of drone images, deep learning (DL) methods were revived and made several outcomes in agricultural applications [5].

Rice is the chief grain crop consumed all over the world, as nearly half of the people in the world consume rice as a main food, and more than 85% is consumed in Asia [6]. To accurately predict the quality of rice and grain yield, exploring increasing amounts of rice seedlings is a main factor for uniform maturity and cultivation density of accurate agriculture. Timely and precise data regarding crop status becomes a significant element for enhancing crop production, which is made through potential RS technologies [7]. Additionally, powerful techniques are vital for using RS data effectively. Previously, substantial research attention was given to CV to enrich crop production. Integrating DL and UAV methods must offer instantaneous data regarding disease/pest attacks, crop status, and soil type, which was not possible at the time of the past millennia [8]. Automatic and precise crop classification utilizing UAV-related DL and RSI approaches indicates a vital task for several smart farming applications, which includes water stress monitoring, crop yield estimation, liquid fertilizers, and precise pesticide spraying, crop surveying, or monitoring [9]. Such tasks resulted in cost reduction minimizing time, and crop production increase offering precious data that must help the agriculturalists to make prompt decisions. In the study, some survey studies inspected the applications of either UAV or different DL techniques in various sectors including agriculture [10].

We present an enhanced tunicate swarm algorithm with a deep learning-based rice seedling classification (ETSADL-RSC) technique. The presented ETSADL-RSC technique examines the UAV images to classify them into two classes: Rice seedlings and arable land. Initially, the quality of the images can be upgraded by contrast limited adaptive histogram equalization (CLAHE) approach. Next, the ETSADL-RSC approach uses the neural architectural search network (NASNet) method for the feature extraction process and its hyperparameters can be tuned by the ETSA model. For the classification of rice seedlings, the ETSADL-RSC approach uses a sparse autoencoder (SAE) model. The experimental result study of the ETSADL-RSC approach is verified on the UAV Rice Seedling Classification dataset.

The rest of the paper is organized as follows. Section 2 provides the related works and Section 3 offers the proposed model. Then, Section 4 gives the result analysis, and Section 5 concludes the paper.

2. Related works

This section offers an insightful exploration of existing research and advancements in the realm of rice seedling classification using DL techniques. Tseng et al. [11] intend to find rice seedlings in the paddy field using transfer learning (TL) from 2 ML methods namely EfficientDet-D0 and Faster R-CNN. In [12], the author gathered thermal infrared and visible images with a UAV or drone. The author establishes a complete rice lodging detection method utilizing SVM and particle swarm optimization (PSO) methods. In [13], RGB color images are taken, and ground truth (GT) pictures are gained by physically labeling pixels in RGB images has 3 separate categories. The class weight coefficient is computed. RGB and GT images are utilized. In [14], the RSI of parental paddy fields is acquired through a multispectral camera in a drone. Six types of noticeable light vegetation indices and 4 types of multispectral vegetation indices are implemented. Desai et al. [15] presented an easy pipeline for identifying areas that cover flowering panicles. The technique depends on image classification utilizing a convolutional neural network (CNN). The author assessed this technique on a five-time series image series of 3 dissimilar crop variations.

Wu et al. [16] introduced a potential approach that utilizes CV to precisely count rice seedlings in digital images. Initially, a drone prepared with RGB cameras is utilized for obtaining field images at the seedling level. In [17], three kinds of ensemble methods including soft voting, model stacking, and hard voting are devised. Such ensemble methods integrated textures extracted from UAV-RGB images, RGB-VIs, color space, and 5 ML models as base methods. Latif et al. [18] devised a DCNN TL-oriented technique for the precise classification and detection of rice leaf disease. The presented methodology involves a modified VGG19-related TL approach. In [19], the InceptionResNetV2 CNN methodology by implementing a TL approach is introduced for the identification of diseases in rice leaf images. Reddy et al. [20] implemented an artificial neural network (ANN) technique, related to present kinetic and isotherm equations. Furthermore, a dedicated user interface was formulated for anticipating barium and strontium elimination depending on the parameters of the sorption process.

Michelini et al. [21] developed a discriminant formula, by utilizing growth and physiological parameters. Another study accentuates a robust association between LT tolerance scores during seedling phases and plant yield at ripening, primarily influenced by panicle weight and the panicle number per plant. In [22], a remedy is introduced by harnessing DL and TL models. Din et al. [23]

presented the "RiceNet" CV model based on the Deep CNN (DCNN) framework. The DL pre-trained methods, particularly InceptionV3 and InceptionResNetV2 approaches are used. The Adam optimizer is used to fine-tune and reduce back-propagation errors. In [24], an information technology system is presented. Feature selection comprised statistical evaluation of features, and classification utilized six morphological factors with five diverse AI models. Kulkarni, and Shastri [25] presented a novel CNN methodology to classify the widely seen rice leaf diseases. Studies leverage ML and DL models like TL for rice seedling and disease detection, employing several data sources like thermal infrared, visible, and RGB images from drones, along with ensemble techniques and artificial neural networks for precise classification in rice-related applications.

Despite the major development complete in the realm of Rice Seedling Classification utilizing DL, a noticeable research gap lies in the inadequate search of hyperparameter tuning techniques. The details of DNN request careful standardization of hyperparameters to improve model generalization and solution. Present works frequently lack complete surveys into the optimum configurations of hyperparameters exact to rice seedling classification tasks. As hyperparameter tuning plays an essential part in perfecting model behavior, addressing this gap becomes vital to solve the full possibility of DL methods in precisely discriminating rice seedling changes. A meticulous examination of hyperparameter tuning plans will not only donate to the modification of model accuracy but also foster a deeper understanding of the degrees inherent in the classification procedure, paving the method for more strong and dependable techniques in agricultural applications.

3. The proposed model

In this study, an automatic rice seedling identification model called the ETSADL-RSC system on UAV images is presented. The presented ETSADL-RSC method majorly aims at the recognition of images into two classes: Rice seedlings and arable land. In the developed ETSADL-RSC approach, several procedures have been involved such as contrast enhancement, NASNet feature extractor, ETSA-based hyperparameter tuning, and SAE classification. Figure 1 defines the working process of the ETSADL-RSC approach.

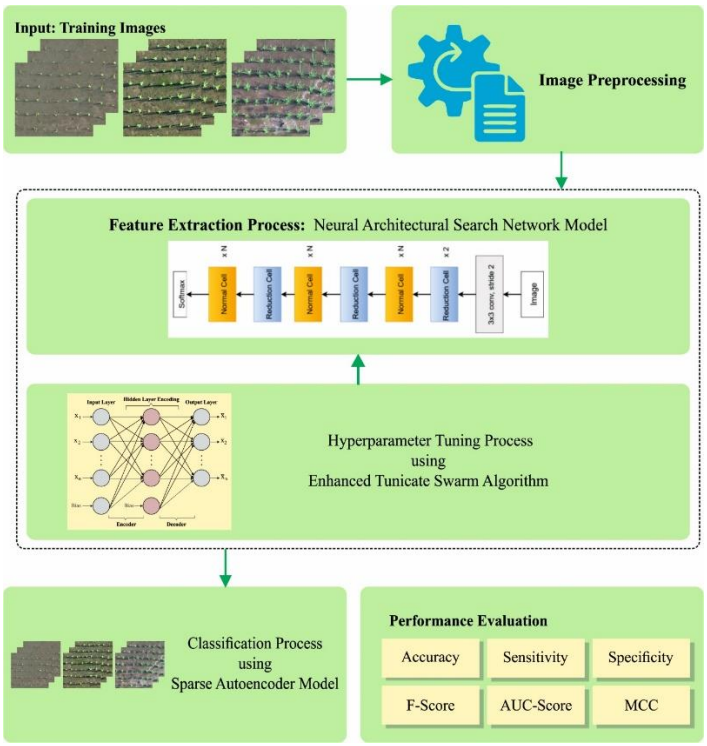

Figure 1. Working procedure of the ETSADL-RSC approach.

3.1. Image pre-processing

In the preliminary phase, the ETSADL-RSC technique enhances the contrast level of the image using the CLAHE technique. The CLAHE technique is formulated dependent upon dividing the images into non-overlapping areas of around equal size [26]. For accomplishing an optimum statistical examination, the count of regions is generally chosen that is equal to 64 by similarly distributing the image by 8 from every direction. This partition affects 3 dissimilar sets of regions. The class of corner regions (CR) includes 4 regions. The class of border region (BR) contains 24 regions. The class of inner region (IR) contains every remaining 36 regions. All the regions on the image border, apart from the CR, go to these classes. During the projected approach, a primary histogram of every region was estimated. Afterward, dependent on the anticipated limit to contrast expansion, the clip limit to clipping histogram was obtained. Then, all the histograms are redistributed thereby height could not exceed the clip limit. Finally, the cumulative distribution function (CDF) of the consequential contrast limited histogram was decided for grayscale mapping. During this approach, pixels can be mapped by linearly taking part in the outcome of the mapping of 4 neighboring regions.

3.2. Feature extraction using NASNet model

To derive a useful set of feature vectors, the NASNet model is used in this work. Google Brain constructs NASNet. They proposed a NASNet to find construction blocks on smaller data and later move the blocks to big data [27]. Also, a regularization technique named Scheduled Drop Path is presented that significantly raises the generalization of NASNet. Last, NASNet architecture achieves

cutting-edge outcomes having lower intricacy and small model size. In the study, the pre-trained NASNet method is used and calculated for different hyperparameters, namely batch size, activation function, optimizer, and so on, that helps to accomplish the maximum accuracy amongst the existing solution with the smallest computation cost. Figure 2 illustrates the structure of the NASNet approach.

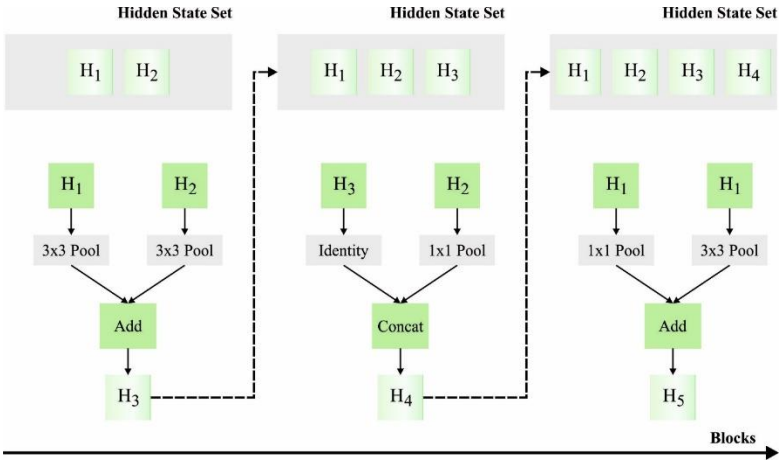

Figure 2. Structure of NASNet.

As introduced by NASNet, the best block is examined by method over reinforcement learning.

N represents the number of motif replications that is a free parameter and the convolutional (Conv) filter at the initial stage is utilized for scaling. This cell is called a reduction and normal cell. A reduction cell executes a process the same as max pooling and returns feature maps that are half the size of inputs in each dimension. A normal cell made Conv operations and returned similar size feature maps as input. The structure of reduction and normal cells is recognized by the controller unit employing a recurrent neural network (RNN).

The controller is an RNN that forecasts the residual framework of reduction and normal cells given the first two hidden states (HS) as follows:

- Initially, HS (hj) is selected from HSs created in the prior block or from present (hi), and prior (hi-1) HSs.
- Next, it involves selecting an alternative HS (hj+1) from the similar option as in the preceding step.
- Then, it chooses a function to be employed on (hj) and (hj+1) HSs
- Lastly, it involves choosing a technique to integrate (hj+1) and (hj). There is a specific operation that is employed by the controller model to find the Conv blocks. The operation allowed in controller RNN are.
  - Identity 1 x 1 Conv
  - 1 x 7 Conv followed by a 7 x 1 Conv filter.
  - 1 x 3 Conv followed by a 3 x 1 Conv filter.
  - 3 x 3 dilated Conv
  - 3 x 3 average pooling
  - Max pooling of 3 x 3, 5 x 5, and 7 x 7 filter sizes.
  - Depthwise separable Conv of 3 x 3, 5 x 5, 7 x 7 filter size

3.3. Hyperparameter tuning

In this phase, the ETSA method has been exploited for automated hyperparameter tuning of the NASNet model. Tunicates are one of the optimistic bio-luminescent animals and produce a blue-green light [28]. Tunicate is the only animal in the ocean that moves with the aid of fluid jets for propulsion and endures with the aid of group behavior and jet propulsion. The TSA principally pretends dual tunicate behaviors such as jet propulsion and swarm intelligence. Jet propulsion behavior mainly depends on the interaction between individuals to accomplish conflict avoidance among individual hunts as well as the advection gravity of deep-sea currents. For jet propulsion behaviors, the tunicates should satisfy three major conditions. Next, the search agents move near the optimum search agent. Then, a safer distance from optimum searching agents is kept. SI deals with upgrading the position of the searching agent optimum solution, which determines the position of the companion via modifications in the neural perspective of water flow around tunicates and companion luminescence and cooperates to collect the position of targeted food sources for cluster foraging. The implementation of TSA can be demonstrated in the following:

The tunicates need to ignore conflicts with other search agents utilizing the "A" vector for performing the jet propulsion behaviour to calculate the new location,

$$A = \frac{G}{M}, \tag{3.1}$$

$$G = c_1 + c_2 - F, \tag{3.2}$$

$$F = 2 \cdot C_3. \tag{3.3}$$

From the expression, G shows the gravity, c_1, c_2, and c_3 signify the randomly generated number within [0,1], F is the velocity of the present, and M is the social force amid search agents. It can be mathematically formulated below.

$$\mathrm{M} = \lfloor Pos_{\min} + c_3(Pos_{\max} - Pos_{\min}) \rfloor. \tag{3.4}$$

In Eq (3.4), $Pos_{\min}$ and $Pos_{\max}$ correspondingly indicate initial and slave velocities of attraction. The searching agent moves to the optimal neighbor afterward avoiding the conflict between neighbors.

$$dpos_t = |P_{best} - rand \cdot x_t| \tag{3.5}$$

In Eq (3.5), $dpos_t$ denotes the distance between a food source and search agents. P_{best} is the position of the food source, viz., optimum position. x_t indicates the present position of the search agent and rand represents the generated value at random within [0 and 1].

Then, the search agent moves to the optimal search agent. This behavior can be mathematically modeled in the following:

$$x_t = \begin{cases} P_{besi}^t + A.dpos_t, rand \geq 0.5, \\ P_{besi}^t - A.dpos_t, rand \leq 0.5. \end{cases} \tag{3.6}$$

In Eq (3.6), P_{best}^t indicates the location of the food source at t-th iterations, viz., optimum location at t-th iterations.

The SI of the tunicate was to upgrade other searching agents through the optimum searching agent position and to constantly upgrade the position of other searching agents by the position of the first two optimum searching agents and it can be conveyed in the below-mentioned formula.

$$x_{t+1} = \frac{x_t + x_{t-1}}{2 + c_1}. \tag{3.7}$$

In Eq (3.7), x_{t-1} is the location of the nearby food source of the preceding generation of tunicate. c_1 shows a randomly generated integer ranging from zero to one.

In TSA, the new position of tunicates is updated depending on social interactions between the tunicates and data related to the better tunicate location. This causes the highest increase in search space [29]. Besides, the divergence of search agents needs to be upheld. Thus, a modified version was presented by developing Lévy flight distribution (LFD) in the TSA. This enhances the diversification search capabilities of TSA and avoids the stagnation probabilities. LFD is developed while keeping the same computation burden and TSA architecture where all the tunicates in every iteration might take the same updating process or take the LFD.

$$T_n^*(m) = \begin{cases} T_n(m) + \sigma \oplus Levy(\beta) & if \frac{I}{\text{Max}} It < rand, \\ SF + A.|SF + rand.T_n(m)| & if\ I/\text{Max}\ It > rand \& rand \geq 0.5, \\ SF - A.|SF - rand.T_n(m)| & if\ I/\text{Max}\ It > rand \& rand < 0.5. \end{cases} \tag{3.8}$$

Here, I is the existing iteration; MaxIt signifies the maximal amount of iterations; σ specifies the step size; $\oplus$ shows entry-wise multiplication, and β denotes LFD co-efficient. The second term in the first part characterizes randomized LFs to arbitrarily generate the new position of tunicate based on random walk:

$$\sigma \oplus Levy(\beta) \approx 0.01 \frac{u}{\frac{1}{|v|^{\beta}}} (T(m) - SF). \tag{3.9}$$

In Eq (3.9), u and v are uniformly distributed random numbers. The steps can be given in the Algorithm 1.

Algorithm 1: Steps involved in TSA
Step 1: Initializing the tunicate population. Step 2: Specify $VT_{\min}$ and $VT_{\max}$ parameters ($VT_{\min} = 1$; $VT_{\max} = 4$), and MaxIt. Step 3: Compute the fitness function (FF) based on every tunicate location. Step 4: Exclude tunicate location with better fitness as a food source. Step 5: Upgrade the position of the tunicate through (3.8). Step6: Remedy any violated control parameter by choosing the nearby limit Step 7: Calculate the FF based on every novel searching location and upgrade the tunicate location when it has fitness. Step 8: Rise the iteration stage by one and if it is not identical to MaxIt, reiterate Steps 5–8. Step 9: Output the optimum solution.

The ETSA manners grow an FF to accomplish the highest outcomes of the classifier. It states an optimistic value for demonstrating a good efficiency of candidate results. In this research, the minimalizing of classifier rate of error is supposed as FF and expressed in Eq (3.10).

$$fitness(x_i) = \frac{No.of\ misclassified\ instances}{Total\ no.of\ instances} \times 100. \tag{3.10}$$

3.4. Rice seedling classification

For rice seedling classification, the ETSADL-RSC technique uses the SAE model. Autoencoder (AE) is an unsupervised 3-layer neural network, involving hidden, input, and output layers (reconstruction layer) [30]. The AE can increasingly convert feature vectors into an abstract feature vector that realizes the non-linear conversion from highest to lowest dimensional data space. The processing method of AE is classified into two phases: Encoder and decoder and they are described in the following:

The encoder process from the input to the hidden layers (HL):

$$H = g_{\theta_1}(X) = \sigma\left(W_{ij}X + \phi_1\right). \tag{3.11}$$

The decoder process from the HL to the output layer:

$$Y = g_{\theta_2}(H) = \sigma\left(W_{jk}H + \phi_2\right). \tag{3.12}$$

From the equation, $X = (x_1, x_2, \ldots, x_n)$ represents the input dataset, $Y = (y_1, y_2, \ldots, y_n)$ denotes the reconstructed vector of input dataset and $H = (h_1, h_2, \ldots, h_m)$ shows low dimensional vector outputs from the HL, $X \in R^n$, $Y \in R^n$, and $H \in R^m$(n indicates dimension of input vector and m denotes count of hidden units). $W_{ij} \in R^{m \times n}$ shows the weight connecting matrices betwixt input and HLs. $W_{jk} \in R^{n \times m}$ indicates the weight connecting matrices between hidden as well as output layers. Figure 3 exhibits the architecture of the SAE method.

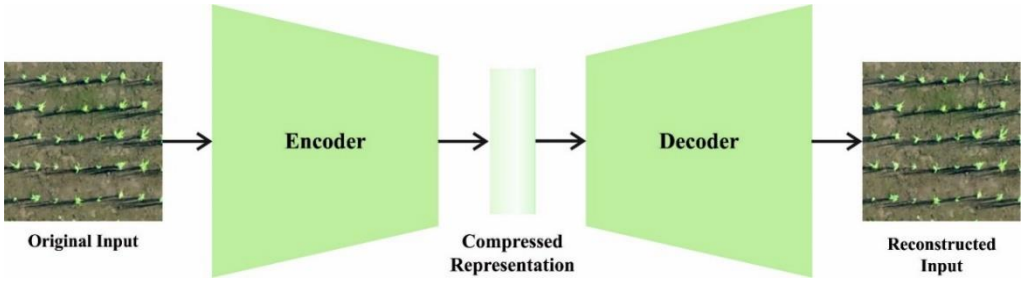

Figure 3. Architecture of SAE.

To accurately reconstruct the input dataset while decreasing resource consumption, $W_{jk} = W_{ij}^T$ exists in this work. $\phi_1 \in R^{n \times 1}$ and $\phi_2 \in R^{m \times 1}$ denote the bias vector of the input and HLs correspondingly. g_{θ_1} and g_{θ_2} represent the HL and output layer correspondingly that aims at mapping

the network summation led to [0,1]. In the proposed algorithm, the sigmoid function can be used as an activation function:

$$g_{\theta_1}(\cdot) = g_{\theta_2}(\cdot) = \frac{1}{1+e^{-x}}. \tag{3.13}$$

The error between the original dataset and the output rebuilt dataset is minimized by adapting the parameter of the encoder and decoder, which implies that AE renovates the original data via training. Consider the output data by HLs was the optimum lowest-dimensional demonstration of original data and involves each data that exists in original data. The reconstructed error function $J_E(W, \phi)$ among H and Y applies the mean squared-error function, where N refers to several input instances.

$$J_E(W, \phi) = \frac{1}{2N}\sum_{r=1}^{N} \| Y^{(r)} - X^{(r)} \|^2. \tag{3.14}$$

The proposed concept of sparse coding to imitate the computation learning of the receptive field of simple cells in the mammalian main visual cortex. Even though the original input dataset is perfectly recovered, the AE does not extract any useful feature in such cases. Thus, the concept of sparse coding presents a sparse drawback term in the HL of AE, so that AE could attain more efficient and concise low-dimensional data features under sparse constraints for expressing the input dataset. Assume that the average activation in the HL is $\hat{\rho}_j, \hat{\rho}_{\mathrm{j}} = \frac{1}{N}\sum_{i=1}^{N}[\, n_j(x_i)]$. The average activation $\hat{\rho}$ approached a constant ρ , which was closer to 0.

Consequently, KL divergence was included as a regularization period of the AE to accomplish the above-mentioned purposes:

$$KL(\rho \| \hat{\rho}) = \rho \log \frac{\rho}{\hat{\rho}_j} + (1-\rho)\log \frac{1-\rho}{1-\hat{\rho}_j}. \tag{3.15}$$

Now, the error function of SAE comprises the mean square error term and the regularization term. It has been demonstrated as follows:

$$J_{sparse}(W, b) = J(W, b) + \mu \sum_{j=1}^{m} K\, L(\rho \| \hat{\rho}_{\mathrm{j}}). \tag{3.16}$$

In Eq (3.16), m represents the number of hidden units, and μ shows the weight factor that controls strength. Moreover, to prevent over-fitting, the weight attenuation item is included in the error function, and λ represents the attenuation coefficient of weight.

$$J_{sparse}(W, b) = J_E(W, b) + \mu \sum_{j=1}^{m} K\, L(\rho \| \hat{\rho}_{\mathrm{j}}) + \frac{\lambda}{2}\sum_{r=1}^{3}\sum_{i=1}^{m}\sum_{j=1}^{m+1}(w_{ij}^{r})^2 \tag{3.17}$$

4. Experimental validation

The proposed model is simulated using Python 3.6.5 tool on PC i5-8600k, GeForce 1050Ti 4GB, 16GB RAM, 250GB SSD, and 1TB HDD.

4.1. Dataset details

In this part, the experimental evaluation of the ETSADL-RSC system takes place using a UAV rice seedling dataset [31]. It comprises 10000 instances with dual classes as given in Table 1. Figure 4 signifies the sample pictures. The parameter settings are provided in the following: learning rate: 0.01, activation: ReLU, epoch count: 50, dropout: 0.5, and size of batch: 5. The dataset comprises 10000 samples with two classes such as rice seedling and arable land. The dataset includes an orthomosaic image which is the image stitched from a series of nadir-like view UAV images. The dataset clipped eight square images with an 8 m × 8 m area, which contains approximately one thousand hills of rice seedlings in each image.

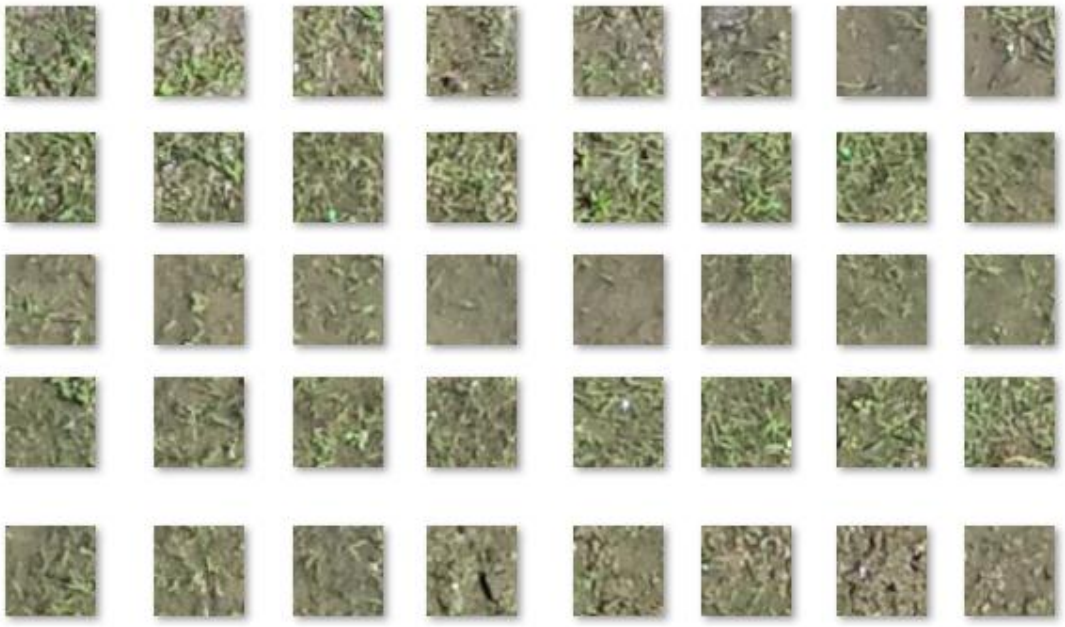

Figure 4. Sample images.

Table 1. Details of the dataset.

Classes	**No. of Instances**
Rice Seedling	5000
Arable land	5000
Total No. of Instances	**10000**

4.2. Results analysis

The confusion matrices of the ETSADL-RSC method on the rice seedling classification process are established in Figure 5. The outcomes designated that the ETSADL-RSC model effectually recognizes the rice seedling and arable land images.

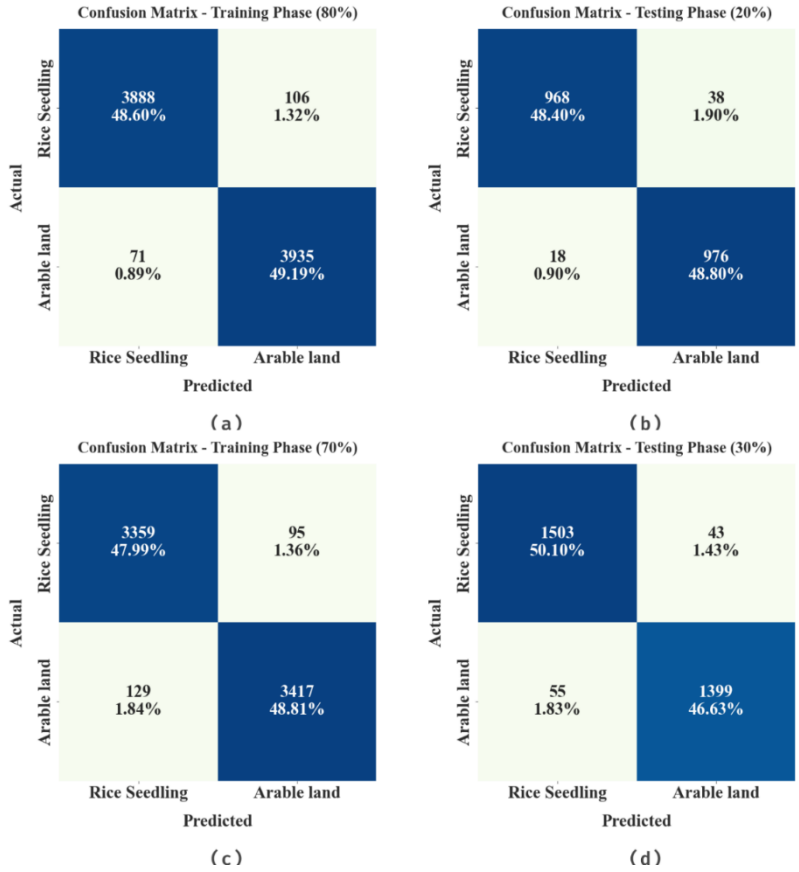

Figure 5. Confusion matrices of the ETSADL-RSC approach. (a and b) TRA and TES databases of 80:20, and (c and d) TRA and TES databases of 70:30.

Table 2. Rice seedling classifier outcome of ETSADL-RSC approach on 80:20 of TRA/TES databases.

Class	$Accuracy_{bal}$	Sensitivity	Specificity	F-Score	AUC Score	MCC
TRA Phase (80%)						
Rice Seedling	97.35	97.35	98.23	97.77	97.79	95.58
Arable land	98.23	98.23	97.35	97.80	97.79	95.58
Average	**97.79**	**97.79**	**97.79**	**97.79**	**97.79**	**95.58**
TES Phase (20%)						
Rice Seedling	96.22	96.22	98.19	97.19	97.21	94.42
Arable land	98.19	98.19	96.22	97.21	97.21	94.42
Average	**97.21**	**97.21**	**97.21**	**97.20**	**97.21**	**94.42**

In Table 2, the overall rice seedling classifier output of the ETSADL-RSC model with 80:20 of TRA/TES databases is given. In Figure 6, a brief rice seedling classification performance of the ETSADL-RSC approach with 80% of the TRA database is given. The results specified that the ETSADL-RSC technique has identifier rice seedlings and arable land effectually. For example, in the rice seedling class, the ETSADL-RSC model has gained $an\ accy_{bal}$ of 97.35%, $sens_y$ of 97.35%, $spec_y$ of 98.23%, a F_{score} of 97.77%, AUC_{score} of 97.79%, and MCC of 95.58%. Also, on arable land

class, the ETSADL-RSC technique has gained an $accy_{bal}$ of 98.23%, $sens_y$ of 98.23%, $spec_y$ of 97.35%, F_{score} of 97.80%, AUC_{score} of 97.79%, and MCC of 95.58%.

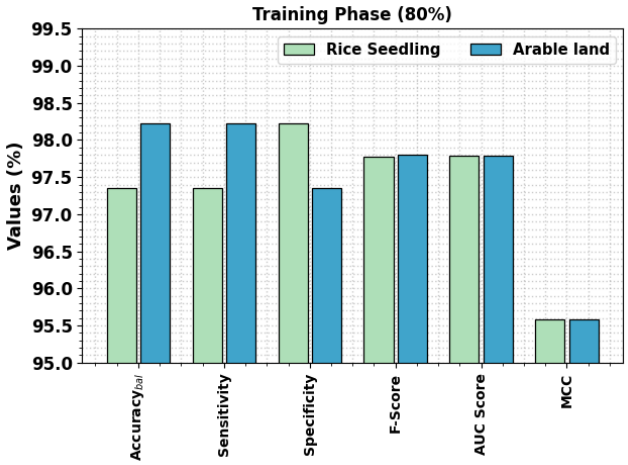

Figure 6. Rice seedling classifier outcome of the ETSADL-RSC approach on 80% of TRA database.

In Figure 7, the detailed rice seedling classification performance of the ETSADL-RSC approach with 20% of the TES database is given. The results exhibited the ETSADL-RSC method has identifier rice seedlings and arable land effectually. For example, in the rice seedling class, the ETSADL-RSC approach has reached an $accy_{bal}$ of 96.22%, $sens_y$ of 96.22%, $spec_y$ of 98.19%, F_{score} of 97.19%, AUC_{score} of 97.21%, and MCC of 94.42%. Similarly, on arable land class, the ETSADL-RSC technique has reached an $accy_{bal}$ of 98.19%, $sens_y$ of 98.19%, $spec_y$ of 96.22%, F_{score} of 97.21%, AUC_{score} of 97.21%, and MCC of 94.42%.

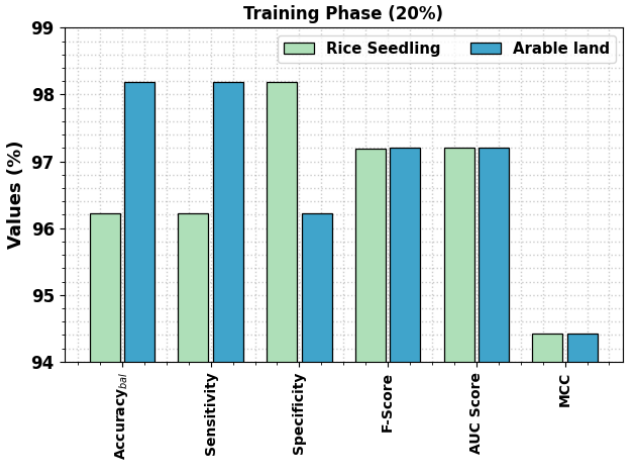

Figure 7. Rice seedling classifier outcome of ETSADL-RSC approach on 20% of TES database.

In Table 3, the complete rice seedling classifier output of the ETSADL-RSC model with 70:30 of TRA/TES databases is given. In Figure 8, a brief rice seedling classification performance of the ETSADL-RSC technique with 70% of the TRA database is given. The results exhibited that the ETSADL-RSC model has identifier rice seedlings and arable land effectually. For example, in the rice seedling class, the ETSADL-RSC method has reached an $accy_{bal}$ of 97.25%, $sens_y$ of 97.25%, $spec_y$ of 96.36%, F_{score} of 96.77%, AUC_{score} of 96.81%, and MCC of 93.60%. Likewise, on arable land class, the ETSADL-RSC technique has gained an $accy_{bal}$ of 96.36%, $sens_y$ of 96.36%, $spec_y$ of 97.25%, F_{score} of 96.83%, AUC_{score} of 96.81%, and MCC of 93.60%.

Table 3. Rice seedling classifier outcome of ETSADL-RSC approach on 70:30 of TRA/TES databases.

Class	$Accuracy_{bal}$	Sensitivity	Specificity	F-Score	AUC Score	MCC
TRA Phase (70%)						
Rice Seedling	97.25	97.25	96.36	96.77	96.81	93.60
Arable land	96.36	96.36	97.25	96.83	96.81	93.60
Average	**96.81**	**96.81**	**96.81**	**96.80**	**96.81**	**93.60**
TES Phase (30%)						
Rice Seedling	97.22	97.22	96.22	96.84	96.72	93.46
Arable land	96.22	96.22	97.22	96.62	96.72	93.46
Average	**96.72**	**96.72**	**96.72**	**96.73**	**96.72**	**93.46**

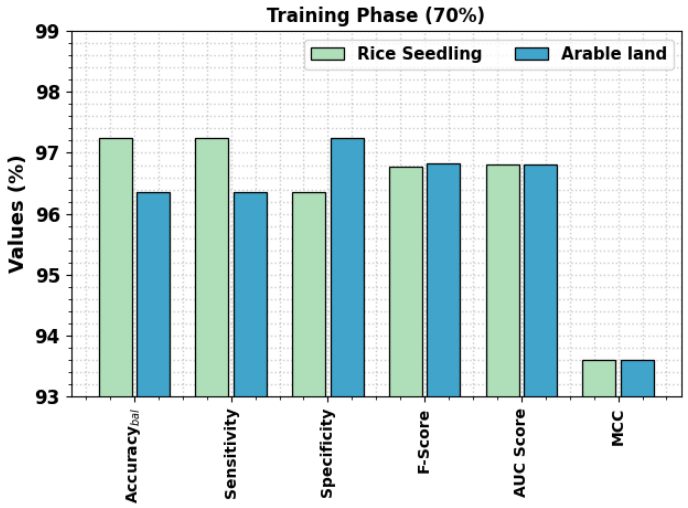

Figure 8. Rice seedling classifier outcome of the ETSADL-RSC approach on 70% of TRA database.

In Figure 9, the detailed rice seedling classification performance of the ETSADL-RSC model with 30% of the TES database is given. The outcomes specified that the ETSADL-RSC technique has identifier rice seedlings and arable land effectually. For example, in the rice seedling class, the ETSADL-RSC technique has gained an $accy_{bal}$ of 97.22%, $sens_y$ of 97.22%, $spec_y$ of 96.22%, F_{score} of 96.84%, AUC_{score} of 96.72%, and MCC of 93.46%. Likewise, on arable land class, the

ETSADL-RSC method has reached an $accy_{bal}$ of 96.22%, $sens_y$ of 96.22%, $spec_y$ of 97.22%, F_{score} of 96.62%, AUC_{score} of 96.72%, and MCC of 93.46%.

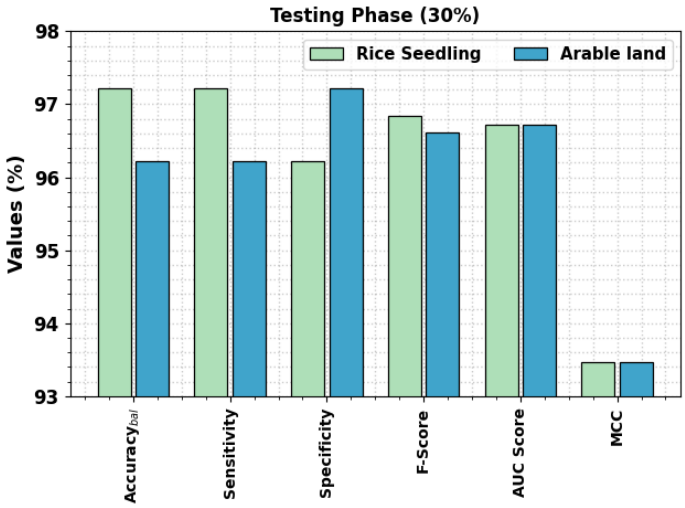

Figure 9. Rice seedling classifier outcome of ETSADL-RSC approach on 30% of TES database.

The TACC and VACC of the ETSADL-RSC method are surveyed on rice seedling classification performance in Figure 10. The figure exhibits that the ETSADL-RSC method has enhanced performance with enlarged values of TACC and VACC. Particularly, the ETSADL-RSC system has extended the greatest TACC results.

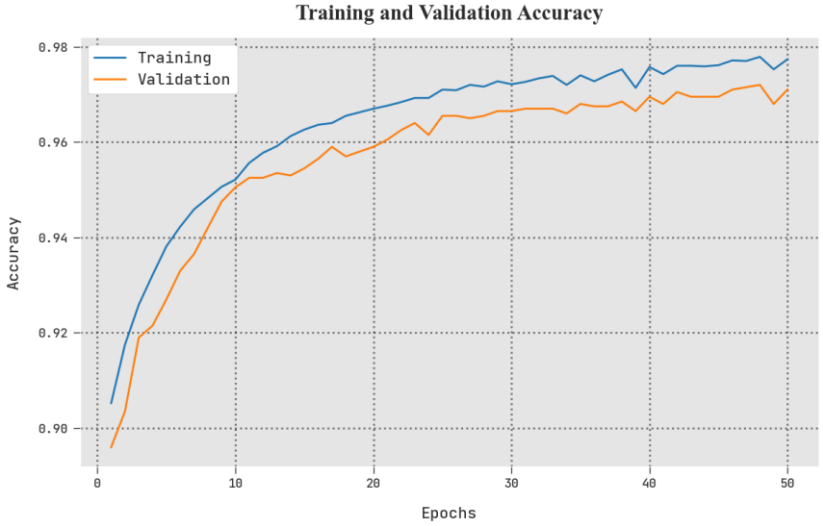

Figure 10. TACC and VACC analyses of ETSADL-RSC approach.

The TLS and VLS of the ETSADL-RSC model are verified for the rice seedling classification performance in Figure 11. The result exhibited that the ETSADL-RSC approach has revealed higher

performance with the smallest values of TLS and VLS. Seemingly, the ETSADL-RSC approach has condensed VLS results.

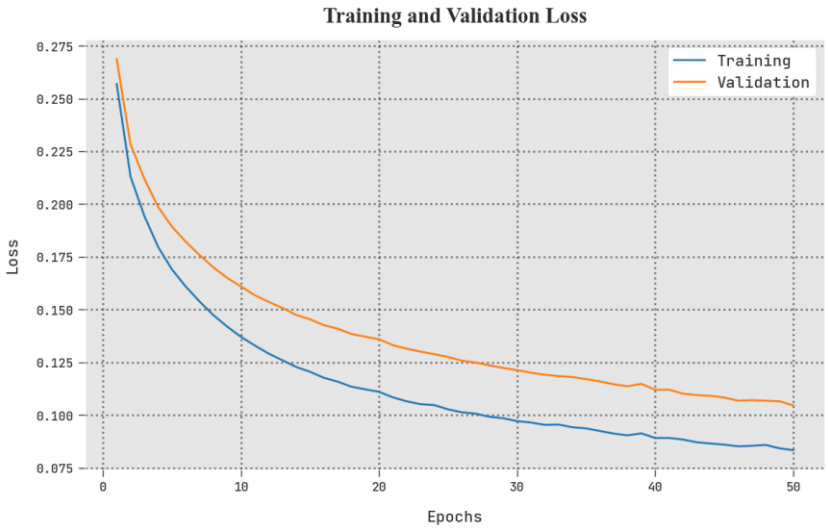

Figure 11. TLS and VLS analyses of ETSADL-RSC approach

A clear precision-recall study of the ETSADL-RSC model in the test dataset is given in Figure 12. The outcomes exhibited that the ETSADL-RSC methodology has upgraded values.

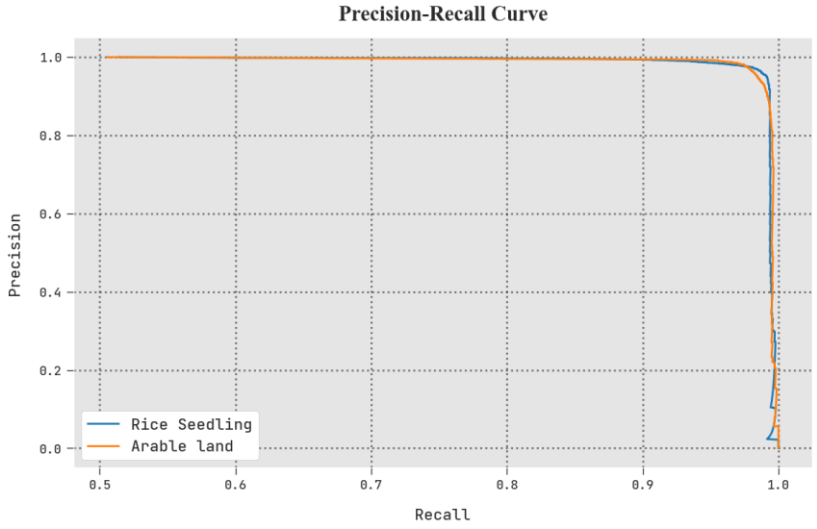

Figure 12. Precision-recall analysis of the ETSADL-RSC model.

The detailed ROC analysis of the ETSADL-RSC method in the test database is shown in Figure 13. The results of the ETSADL-RSC model revealed its ability to categorize different classes below the test database.

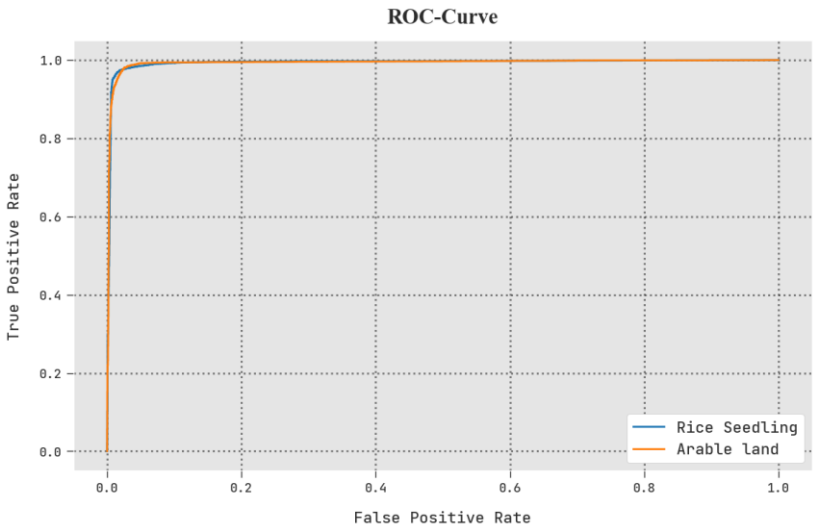

Figure 13. ROC curve analysis of the ETSADL-RSC approach.

In Table 4, a detailed classification result of the ETSADL-RSC method with recent approaches is provided. Figure 14 exhibits a comparative $accu_y$ of the ETSADL-RSC approach with current systems. The experimental outcomes stated that the SGD method and XGBoost model have reached an $accu_y$ of 91.61% and 92.47% respectively. In contrast, the GNB, ELM, KELM, RF, and SVM models have achieved closer $accu_y$ values of 95.96%, 95.34%, 93.72%, 95%, and 96.42%. However, the ETSADL-RSC method exhibited a higher $accu_y$ of 97.79%.

Table 4. Comparative analysis of the ETSADL-RSC method with recent approaches.

Methods	Accuracy	Sensitivity	Specificity	F-Score
ETSADL-RSC	97.79	97.79	97.79	97.79
SGD	91.61	92.75	91.38	93.76
GNB	95.96	94.85	95.32	95.89
ELM	95.34	93.78	95.58	93.07
KELM	93.72	94.57	93.34	93.13
XgBoost	92.47	95.97	92.10	95.14
RF	95.00	94.05	94.44	95.58
SVM	96.42	94.64	93.39	94.97

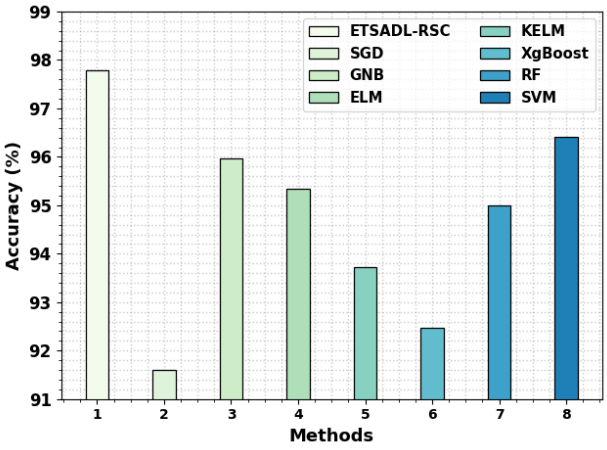

Figure 14. $Accu_y$ analysis of the ETSADL-RSC approach with recent techniques.

Figure 15 shows a detailed $sens_y$ review of the ETSADL-RSC method with recent techniques. The simulation values depict that the SGD method and XGBoost technique has reached a reduced $sens_y$ of 92.75% and 95.97% correspondingly. In Contrast, the GNB, ELM, KELM, RF, and SVM methodologies have closer $sens_y$ values of 94.85%, 93.78%, 94.57%, 94.05%, and 94.64% correspondingly. However, the ETSADL-RSC approach has shown maximum performance with a $sens_y$ of 97.79%.

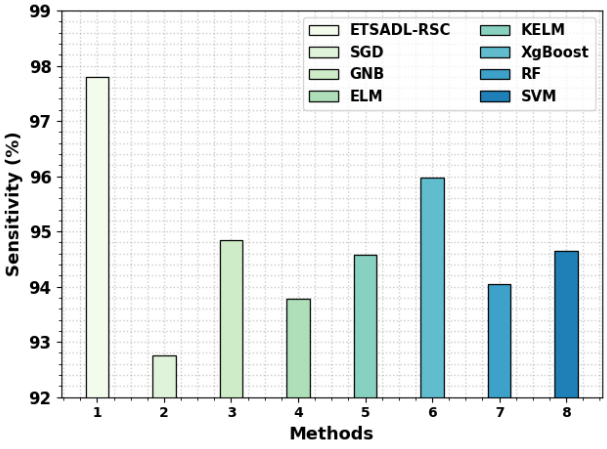

Figure 15. $Sens_y$ analysis of the ETSADL-RSC approach with recent approaches.

Figure 16 exhibited a brief $spec_y$ study of the ETSADL-RSC system with current techniques. The simulation values designated that the SGD approach and XGBoost algorithm have gained decreased $spec_y$ of 91.38% and 92.10% correspondingly. Contrastingly, the GNB, ELM, KELM, RF, and SVM methods have accomplished closer $spec_y$ values of 95.32%, 95.58%, 93.34%, 94.44%, and 93.39% correspondingly. But the ETSADL-RSC approach has shown maximum performance with $spec_y$ of 97.79%.

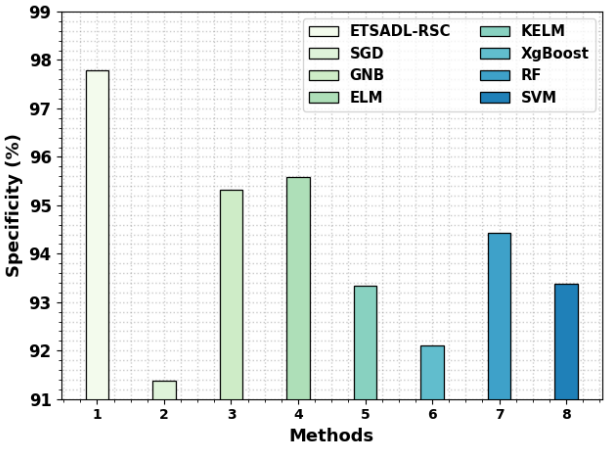

Figure 16. $Spec_y$ analysis of ETSADL-RSC approach with recent approaches.

Figure 17 exhibits a comparative F_{score} study of the ETSADL-RSC technique with current methods. The results exhibit that the SGD method and XGBoost technique have reached reduced F_{score} of 93.76% and 95.14% correspondingly. In Contrast, the GNB, ELM, KELM, RF, and SVM algorithms have accomplished closer F_{score} values of 95.89%, 93.07%, 93.13%, 95.58%, and 94.97% correspondingly. However, the ETSADL-RSC technique has shown the highest performance with an F_{score} of 97.79%. These outcomes emphasized the superior performance of the ETSADL-RSC technique.

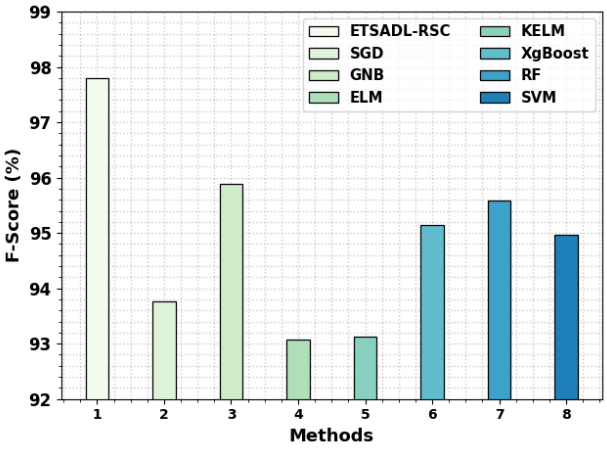

Figure 17. F_{score} analysis of ETSADL-RSC approach with recent algorithms.

5. Conclusions

In this research, an automatic rice seedling classification system termed the ETSADL-RSC system on UAV images is presented. The presented ETSADL-RSC technique aims at the recognition of images into two classes: Rice seedlings and arable land. At an early stage, image excellence can be improved using the CLAHE technique. Then, the ETSADL-RSC technique exploited the NASNet

method for the feature extraction process and its hyperparameters can be tuned by the ETSA model. For rice seedling classification, the ETSADL-RSC approach used the SAE model. The experimental outcome of the ETSADL-RSC system has been verified for the UAV Rice Seedling Classification dataset. Extensive simulation analysis of the ETSADL-RSC model stated the greater accuracy performance of 97.79% over other DL classifiers. The ETSADL-RSC technique's limitations may include potential challenges in handling diverse environmental conditions. In the future, a hybrid DL classification system will be considered to enhance the solution of the ETSADL-RSC approach.

In the future, evolving the area of Rice Seedling Classification utilizing DL offers exciting opportunities for further invention. The search of new deep neural network architectures personalized exactly for the particulars of rice seedling features stays a promising avenue. Incorporating advanced models such as transfer learning and area adaptation could improve model generalization through different environmental states and databases. Moreover, the combination of multi-modal data, with spectral and temporal data, could deliver a more complete understanding of rice seedling features, further enlightening classification accuracy. Also, study efforts must be directed near the growth of interpretable methods, simplifying not only exact predictions but also perceptive decision-making in farming practices.

Use of AI tools declaration

The authors declare they have not used Artificial Intelligence (AI) tools in the creation of this article.

Acknowledgments

The authors extend their appreciation to the Deanship of Scientific Research at King Khalid University for funding this work through a large group Research Project under grant number (RGP2/35 /44). Princess Nourah bint Abdulrahman University Researchers Supporting Project number (PNURSP2024R330), Princess Nourah bint Abdulrahman University, Riyadh, Saudi Arabia. This study is partially funded by the Future University in Egypt (FUE).

Conflict of interest

The authors declare that they have no conflicts of interest. The manuscript was written through the contributions of all authors. All authors have approved the final version of the manuscript.

References

1. M. D. Yang, H. H. Tseng, Y. C. Hsu, C. Y. Yang, M. H. Lai, D. H. Wu, A UAV open dataset of rice paddies for deep learning practice, *Remote Sens.*, **13** (2021), 1358. https://doi.org/10.3390/rs13071358

2. Q. Yang, L. Shi, J. Han, J. Yu, K. Huang, A near real-time deep learning approach for detecting rice phenology based on UAV images, *Agr. Forest Meteorol.*, **287** (2020), 107938. https://doi.org/10.1016/j.agrformet.2020.107938
3. V. Margapuri, N. Penumajji, M. Neilsen, Seed classification using synthetic image datasets generated from low-altitude UAV imagery, In: *2021 20th IEEE International Conference on Machine Learning and Applications (ICMLA)*, 2021, 116–121. https://doi.org/10.1109/ICMLA52953.2021.00026
4. K. Dilmurat, V. Sagan, M. Maimaitijiang, S. Moose, F. B. Fritschi, Estimating crop seed composition using machine learning from multisensory UAV data, *Remote Sens.*, **14** (2022), 4786. https://doi.org/10.3390/rs14194786
5. M. M. Anuar, A. A. Halin, T. Perumal, B. Kalantar, Aerial imagery paddy seedlings inspection using deep learning, *Remote Sens.*, **14** (2022), 274. https://doi.org/10.3390/rs14020274
6. A. O. Conrad, W. Li, D. Y. Lee, G. L. Wang, L. Rodriguez-Saona, P. Bonello, Machine learning-based presymptomatic detection of rice sheath blight using spectral profiles, *Plant Phenomics*, **2020** (2020), 8954085. https://doi.org/10.34133/2020/8954085
7. S. Tan, J. Liu, H. Lu, M. Lan, J. Yu, G. Liao, et al., Machine learning approaches for rice seedling growth stages detection, *Front. Plant Sci.*, **13** (2022), 914771. https://doi.org/10.3389/fpls.2022.914771
8. F. Liao, X. Feng, Z. Li, D. Wang, C. Xu, G. Chu, et al., A spatio-temporal convolutional neural network model for rice nutrient level diagnosis at rice panicle initiation stage, http://doi.org/10.2139/ssrn.4272680
9. F. M. Muharam, K. Nurulhuda, Z. Zulkafli, M. A. Tarmizi, A. N. H. Abdullah, M. F. Che Hashim, et al., UAV-and Random-Forest-AdaBoost (RFA)-based estimation of rice plant traits, *Agronomy*, **11** (2021), 915. https://doi.org/10.3390/agronomy11050915
10. T. Yamaguchi, Y. Tanaka, Y. Imachi, M. Yamashita, K. Katsura, Feasibility of combining deep learning and RGB images obtained by unmanned aerial vehicle for leaf area index estimation in rice, *Remote Sens.*, **13** (2021), 84. https://doi.org/10.3390/rs13010084
11. H. H. Tseng, M. D. Yang, R. Saminathan, Y. C. Hsu, C. Y. Yang, D. H. Wu, Rice seedling detection in UAV images using transfer learning and machine learning, *Remote Sens.*, **14** (2022), 2837. https://doi.org/10.3390/rs14122837
12. T. Liu, R. Li, X. Zhong, M. Jiang, X. Jin, P. Zhou, et al., Estimates of rice lodging using indices derived from UAV visible and thermal infrared images, *Agr. Forest Meteorol.*, **252** (2018), 144–154. https://doi.org/10.1016/j.agrformet.2018.01.021
13. X. Ma, X. Deng, L. Qi, Y. Jiang, H. Li, Y. Wang, et al., Fully convolutional network for rice seedling and weed image segmentation at the seedling stage in paddy fields, *PloS One*, **14** (2019), e0215676. https://doi.org/10.1371/journal.pone.0215676
14. H. Liu, Y. Qi, W. Xiao, H. Tian, D. Zhao, K. Zhang, et al., Identification of male and female parents for hybrid rice seed production using UAV-based multispectral imagery, *Agriculture*, **12** (2022), 1005. https://doi.org/10.3390/agriculture12071005
15. S. V. Desai, V. N. Balasubramanian, T. Fukatsu, S. Ninomiya, W. Guo, Automatic estimation of heading date of paddy rice using deep learning, *Plant Methods*, **15** (2019), 76. https://doi.org/10.1186/s13007-019-0457-1

16. J. Wu, G. Yang, X. Yang, B. Xu, L. Han, Y. Zhu, Automatic counting of in situ rice seedlings from UAV images based on a deep fully convolutional neural network, *Remote Sens.*, **11** (2019), 691. https://doi.org/10.3390/rs11060691
17. H. Ge, F. Ma, Z. Li, Z. Tan, C. Du, Improved accuracy of phenological detection in rice breeding by using ensemble models of machine learning based on UAV-RGB imagery, *Remote Sens.*, **13** (2021), 2678. https://doi.org/10.3390/rs13142678
18. G. Latif, S. E. Abdelhamid, R. E. Mallouhy, J. Alghazo, Z. A. Kazimi, Deep learning utilization in agriculture: Detection of rice plant diseases using an improved CNN model, *Plants*, **11** (2022), 2230. https://doi.org/10.3390/plants11172230
19. N. Krishnamoorthy, L. V. N. Prasad, C. S. P. Kumar, B. Subedi, H. B. Abraha, V. E. Sathishkumar, Rice leaf diseases prediction using deep neural networks with transfer learning, *Environm. Res.*, **198** (2021), 111275. https://doi.org/10.1016/j.envres.2021.111275
20. B. S. Reddy, A. K. Maurya, V. E. Sathishkumar, P. L. Narayana, M. H. Reddy, A. Baazeem, et al., Prediction of batch sorption of barium and strontium from saline water, *Environ. Res.*, **197** (2021), 111107. https://doi.org/10.1016/j.envres.2021.111107
21. M. C. Michelini, A. Gazquez, M. L. Checovich, A. S. Tamayo, S. J. Maiale, A. B. Menéndez, et al., Determination of low-temperature stress during the vegetative stage as a tool to predict plant yield in rice genotypes with contrasting tolerance levels, *J. Agron. Crop Sci.*, **210** (2024), e12670. https://doi.org/10.1111/jac.12670
22. P. I. Ritharson, K. Raimond, X. A. Mary, J. E. Robert, J. Andrew, DeepRice: A deep learning and deep feature based classification of Rice leaf disease subtypes, *Artif. Intell. Agric.*, **11** (2024), 34–49. https://doi.org/10.1016/j.aiia.2023.11.001
23. N. M. U. Din, A. Assad, R. A. Dar, M. Rasool, S. U. Sabha, T. Majeed, et al., RiceNet: A deep convolutional neural network approach for classification of rice varieties, *Expert Syst. Appl.*, **235** (2024), 121214. https://doi.org/10.1016/j.eswa.2023.121214
24. G. Çınarer, N. Erbaş, A. Öcal, Rice classification and quality detection success with artificial intelligence technologies, *Braz. Arch. Biol. Technol.*, **67** (2024), e24220754. https://doi.org/10.1590/1678-4324-2024220754
25. P. Kulkarni, S. Shastri. Rice leaf diseases detection using machine learning, *J. Sci. Res. Technol.*, **2** (2024), 17–22. https://doi.org/10.61808/jsrt81
26. H. M. Qassim, N. M. Basheer, M. N. Farhan, Brightness preserving enhancement for dental digital X-ray images based on entropy and histogram analysis, *J. Appl. Sci. Eng.*, **22** (2019), 187–194. https://doi.org/10.6180/jase.201903_22(1).0019
27. S. Nalluri, R. Sasikala, A deep neural architecture for SOTA pneumonia detection from chest X-rays, *Int. J. Syst. Assur. Eng. Manag.*, **15** (2024), 489–502. https://doi.org/10.1007/s13198-022-01788-x
28. Y. Zhang, Q. He, L. Yang, C. Liu, An improved tunicate swarm algorithm for solving the multiObjective optimisation problem of airport gate assignments, *Appl. Sci.*, **12** (2022), 8203. https://doi.org/10.3390/app12168203
29. T. Fetouh, A. M. Elsayed, Optimal control and operation of fully automated distribution networks using improved tunicate swarm intelligent algorithm, *IEEE Access*, **8** (2020), 129689–129708. https://doi.org/10.1109/ACCESS.2020.3009113

30. B. Yan, G. Han, Effective feature extraction via stacked sparse autoencoder to improve intrusion detection system, *IEEE Access*, **6** (2018), 41238–41248. https://doi.org/10.1109/ACCESS.2018.2858277
31. Rice Seedling Dataset, Available from: https://github.com/aipal-chu/RiceSeedlingDataset.

AIMS Press

© 2024 the Author(s), licensee AIMS Press. This is an open access article distributed under the terms of the Creative Commons Attribution License (http://creativecommons.org/licenses/by/4.0)